J. Fluid Mech. (1977), *vol.* 82, *part* 4, *pp.* 621–641
Printed in Great Britain

The excitation of damped waves diffracted over a submerged circular sill

By H. D. PITE

School of Mathematical Sciences, New South Wales Institute of Technology, Broadway, New South Wales 2007, Australia

(Received 14 April 1975 and in revised form 31 March 1977)

A mathematical model of rectilinear surface waves incident on a submerged circular sill is developed. The class of waves considered consists of those for which the ratio of wavelength to water depth is large but which do not necessarily belong in the long-wave category. A friction damping term is introduced into the equations of motion and the solutions obtained for the regions over the sill and in the ocean are matched by assuming a continuous surface and energy flux at the sill edge. The results show large reductions in the Q-factor of the resonance peaks brought about by friction damping. It is also found that, except at low frequency, a large number of overlapping resonance peaks which are out of phase with one another occupy a relatively narrow frequency band such that these resonance peaks effectively cancel one another. Experiments were performed to determine the friction constant used in the equations of motion and, using this friction constant, the theoretical results of wave resonance are verified.

1. Introduction

The problem dealt with in this paper is that of a continuous train of frictionally damped surface waves incident on a submerged circular sill situated in a non-rotating unbounded ocean. A portion of the incident wave energy is scattered at the sill edge and the remaining portion is transmitted onto the sill. Once over the sill the waves undergo multiple partial reflexions at the sill edge and, in doing so, scatter some of their energy to infinity. It has been shown for circular symmetry (Longuet-Higgins 1967) that even if friction is neglected there is always some loss of energy from the sill to infinity although this loss may be very small. The response coefficients for frictionless long waves have been derived by Longuet-Higgins (1967) and show the possibility of large amplification over the sill for certain frequencies, the wave energy in these instances being said to be nearly trapped. Subsequent work by Summerfield (1969) was carried out with a circular island shelf model and an elliptical sill model. Many others have investigated the amplitude response due to step-type changes in the bathymetry in the ocean; an extensive survey of the literature of this subject is presented by Summerfield (1969). In many cases of theoretical work in this field the waves were considered to be in the long-wave region. With this proviso it was satisfactory to impose, at the depth discontinuity, the conditions of a continuous surface streamline and a continuous mass flux, the latter being evaluated by assuming a discontinuous horizontal particle velocity at the sill edge. But when long-wave theory is not valid, these conditions give the physically unsatisfactory result that more energy is being

carried away from the step by the transmitted and reflected waves than is arriving at it. To eliminate this inconsistency the mass flux condition was replaced by an energy flux condition. Section 4 deals in more detail with this choice of matching conditions at the discontinuity.

In almost all cases where waves lie in the intermediate-to-long class, the effect of friction will be of considerable importance; this will be especially so if the system being examined is a resonant one. A linear friction term is introduced (§ 2) into the equations of motion and an associated potential function is deduced (§ 3). The linear friction coefficient for the model studies is found from direct measurement of wave decay in the laboratory.

As waves pass over a depth discontinuity there will be some loss of energy due to flow separation. Experiments on a one-dimensional shelf by Pite (1973) showed that this loss was significant when the incident waves progressed from the shallow to the deep water, but for incident waves travelling in the opposite direction no evidence of energy loss was apparent. In the former instance, where there were energy losses, the reflected wave amplitudes agreed, within the experimental limitations, with the predicted ones whereas the transmitted wave amplitudes were, on the average, smaller than the theoretical ones by about 7 %. It therefore appears from these experimental results that the extraneous losses near the sill edge will affect primarily the scattered wave and have a small effect on the waves over the sill.

For the range of wave periods tested and using a depth of 0·84 cm it is found in § 7.1 that the minimum value for the decay coefficient is about 5×10^{-3} cm^{-1}. Therefore a wave travelling a distance equal to the sill diameter of 45·7 cm would undergo a reduction in amplitude due to friction of about 23 % with a corresponding energy loss of 40 %. For the maximum value of this decay coefficient found in § 7.1, the energy loss would be approximately 80 %. In view of these rather high frictional losses found in this experiment it appears reasonable to ignore the energy lost from the waves over the sill to the secondary motion near the sill edge. The wavelength corresponding to the minimum decay was about 63·0 cm and that corresponding to the maximum about 11·5 cm. In other circumstances where the dissipation is much less it is probable that the energy losses near the sill edge will gain importance; in these cases response coefficients calculated in § 5 will not give an adequate description of the wave motion.

Response coefficients are found in § 5 for the waves generated over the sill and for those scattered away from the sill edge. The experimental verification of some of these theoretical results is described in § 7 and in general shows good agreement.

2. The linear friction term

An approach to modelling the bottom friction whilst still retaining linear equations and irrotational motion is to assume that the bottom friction may be replaced by a distributed body force directly proportional to the near-bottom velocity. This approach must, however, be regarded as a first approximation. For the case where there are small motions and the friction coefficient depends only upon viscosity there appear in the literature a number of linear theories (for example Hough 1897; Biesel 1949) which give a description of the fluid motion both inside and outside the boundary layer. In large-scale oceanographic work the friction term is usually considered to be proportional to the square of the near-bottom velocity and any details of motion in the

generally turbulent dissipative layer near the bottom is ignored. This quadratic resistance term may be linearized by replacing it with the product of the near-bottom velocity and a suitably chosen constant (see, for example, Ippen & Harleman 1960). In this study, the linear friction constant is determined experimentally and the details of motion in the rotational bottom layer are ignored.

3. The equations of motion

A non-rotating co-ordinate system is considered in which the vertical co-ordinate z will be directed positive upwards and have its origin on the still water surface. The horizontal co-ordinates will be designated as $\mathbf{x} = (x, y)$ in Cartesian co-ordinates or as $\mathbf{x} = (r, \theta)$ in polar co-ordinates. Departures from the undisturbed water surface will be denoted by $\eta(\mathbf{x}, t)$ and it will be required that these are very much less than the fluid depth h or, more correctly, that the second-order term in the Stokes expansion is much less than the first such that the small amplitude approximation may be used.

The frictional force is modelled empirically as a body force per unit mass: $cu_b h^{-1}$, where $u_b(\mathbf{x}, t)$ is the horizontal particle velocity near the bottom and c is a linear friction coefficient. This coefficient varies with the wave period since the period influences the thickness of the boundary layer (Li 1954) and hence the amount of dissipation per unit time. This dependence on the frequency does not appear in the theoretical development but is determined experimentally.

The equation of motion for this model over a horizontal bed is

$$\partial \mathbf{u}/\partial t = -\rho^{-1}\nabla p - \mathbf{F} - \mathbf{g}, \tag{1}$$

where ρ is the fluid density, $\mathbf{g}$ is the acceleration due to gravity, p is the pressure, $\mathbf{u}$ is the particle velocity and $\mathbf{F}$ is the friction force. It is assumed that there exists a potential function such that

$$(a)\ \nabla^2\phi_c = 0 \tag{2}$$

and

$$(b)\ \nabla\phi_c = \mathbf{u}, \tag{3}$$

where the subscript c refers to a complex quantity of which only the real part is of physical significance.

Using (3) in (1) and integrating with respect to $\mathbf{x}$ yields the integrated Bernoulli equation:

$$\frac{\partial\phi_c}{\partial t} + \frac{p}{\rho} + \frac{c}{h}(\phi_c)_b + gz = 0, \tag{4a}$$

which at the free surface becomes

$$\frac{\partial\phi_c}{\partial t} + \frac{c}{h}(\phi_c)_b + g\eta = 0. \tag{4b}$$

The vertical particle velocity at the free surface is

$$w|_{z=\eta} = \left.\frac{dz}{dt}\right|_{z=\eta} \simeq \left.\frac{\partial\eta}{\partial t}\right|_{z=\eta}.$$

It follows from (3) that $w = \partial\phi_c/\partial z$. Thus the kinematic boundary condition at the free surface is

$$[\partial\phi_c/\partial z]_{z=\eta} \simeq \partial\eta/\partial t. \tag{5}$$

At the bottom there is no vertical velocity so

$$[\partial\phi_c/\partial z]_{z=-h} = 0. \tag{6}$$

Assuming that the potential function can be written as a product of the form

$$\phi_c = f(z)\,\Phi(\mathbf{x})\,e^{-i\sigma t}$$

which is harmonic with time and using (4*b*), (5) and (6) yields a solution of (3) as

$$\phi_c = \frac{i\sigma A' \cosh K(z+h)}{K \sinh Kh}\,\Phi(\mathbf{x})\,e^{-i\sigma t}, \tag{7}$$

where K and A' are constants.

In the case where the wave crests propagate from left to right and are parallel to the y axis, the potential function is

$$\phi_c = \frac{i\sigma A \cosh K(z+h)}{K \sinh Kh}\,e^{i(Kx-\sigma t)}. \tag{8}$$

In physical problems involving circular symmetry, the solution can be written as

$$\phi_c = \frac{i\sigma \cosh K(z+h)}{K \sinh Kh} \sum_{n=0}^{\infty} \{A_n H_n^{(1)}(Kr) + B_n H_n^{(2)}(Kr)\} \cos n\theta\, e^{-i\sigma t}, \quad Kr \neq 0. \tag{9}$$

If the origin is included then a solution is

$$\phi_c = \frac{i\sigma \cosh K(z+h)}{K \sinh Kh} \sum_{n=0}^{\infty} A_n J_n(Kr) \cos n\theta\, e^{-i\sigma t}. \tag{10}$$

The complex 'wavenumber' $K = k + i\alpha$ is evaluated by replacing ϕ_c in (4*b*) with the right-hand side of (7), which gives the wavenumber

$$k = \frac{\sigma^2}{2g}\left\{\frac{\sinh 2kh + (2c/\sigma h)\cosh kh \sin \alpha h}{\sinh^2 kh + \sin^2 \alpha h}\right\} \tag{11}$$

and the decay coefficient

$$\alpha = \frac{\sigma^2}{2g}\left\{\frac{-\sin \alpha h + (2c/\sigma h)\sin kh \cos \alpha h}{\sinh^2 kh + \sin^2 \alpha h}\right\}. \tag{12}$$

4. The matching condition at the depth discontinuity

The partial reflexion of inviscid surface waves incident normally on a step-type depth discontinuity has been investigated by Lamb (1932), Bartholomeusz (1958), Le Mehaute (1960), Newman (1965), Ippen (1966), Miles (1967), Hilaly (1967) and Smith & Sprinks (1975) among others. For the special case of long waves they all obtained the same results for the reflexion and transmission coefficients. However, in many problems involving surface waves, the waves do not belong to this long-wave class. In particular, for the laboratory verification of wave trapping over a sill, as was carried out in this study, it was found difficult to devise an experimental set-up such that the waves were all in the strictly long-wave category. The value of kh used here ranged from 0·08 to 0·31 for the waves over the sill and from 0·16 to 0·65 for the waves in the 'ocean'.

To avoid the mathematical complexities involved in solving the complete boundary-value problem an approximate solution was obtained by ignoring any details of motion near the sill edge. If, as in all the above theories, there are assumed to be no energy

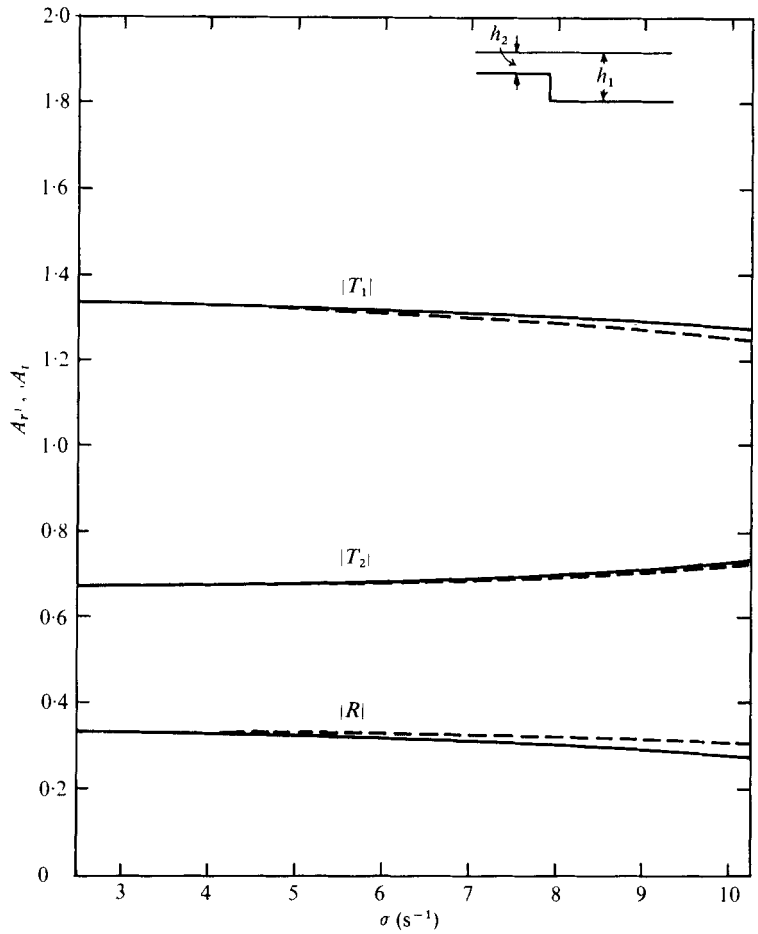

FIGURE 1. Comparison of the transmitted and reflected wave amplitudes with reference to an incident wave of unit amplitude. ——, using Miles' variational solution; – – – –, assuming continuity of surface elevation and energy flux at the step. $|T_1|$, $|T_2|$ = transmitted wave amplitude, incident wave from right, left; $|R|$ = reflected wave amplitude, $|R_1| = |R_2| \equiv |R|$. $h_2/h_1 = \frac{1}{2}$, $h_2 = 0{\cdot}84$ cm.

losses at the discontinuity then the incident energy flux must equal the sum of the reflected and transmitted energy fluxes when averaged over one wave period. The first matching condition was to assume that the instantaneous energy flux is continuous at the step; this was found to yield a solution which conserved the time-average energy flux.

Following all the above authors except Le Mehaute (1960), the second matching condition was the assumption that the surface is a continuous streamline. The condition of a continuous mass flux was not used since, except for long waves in the shallow region, these solutions were in poor agreement with Newman's (1965) results.

Evaluation of the transmission and reflexion coefficients for a step discontinuity using the continuous surface and energy conditions was carried out for various sets of parameters and the results compared with more accurate results computed using Miles' (1967) variational technique. These calculations showed that if both depths are

very small compared with the wavelength then the two solutions coincide and are identical to Lamb's (1932) and Bartholomeusz's (1958) results. Figure 1 shows a comparison between the results from the approximate solution and the variational one using a range of parameters corresponding to the ones used in the experiments. The good agreement between these two sets of results is explained by examining the exponential factor in the exact formulation of the local disturbance (Bartholomeusz 1958). For moderately long waves ($kh \leqslant 0{\cdot}7$) this factor is less than about

$$\exp(-3|x|h^{-1})$$

thus the standing-wave disturbance is confined to a small (compared with the wavelength) region near the step. Therefore, as remarked by Miles (1967), it is reasonable in this case to take the local disturbance as confined to an infinitesimal section near the step and thus, as was done here, to match the continuity conditions at the step. Owing to the small horizontal extent of the local disturbance at the sill edge in comparison with the diameter of the sill used in the experiments, as well as to the agreement between the solutions shown in figure 1 for the step, it was thought justified to use these approximate matching conditions at the edge of the circular sill.

5. The excitation of waves over a submerged circular sill

A circular sill of radius R is taken to be centred at the origin with a water depth above it of h_2. A region, called the ocean, of infinite extent outside the sill has a constant depth of h_1. Sinusoidal plane waves with unit amplitude along $x = 0$ are incident from the ocean and travel in the direction of increasing x. The potential function for these waves is given by (8):

$$(\phi_i)_c = f_1(z)\exp[i(K_1 x - \sigma t)],$$

where a subscript 1 refers to properties pertaining to the ocean and a subscript i refers to the incident wave. Transforming to polar co-ordinates $x = r\cos\theta$ and using a well-known identity involving cylindrical functions gives

$$(\phi_i)_c = f_1(z)\,e^{-i\sigma t}\sum_{n=0}^{\infty}\epsilon_n i^n J_n(K_1 r)\cos n\theta, \tag{13}$$

where $\epsilon_0 = 1$ and $\epsilon_n = 2$ for $n \geqslant 1$.

Upon reaching the sill edge some of the wave energy is scattered and some is transmitted across the sill to undergo multiple partial reflexions at the sill edge. It has been shown for circular symmetry (Longuet-Higgins 1967) that there is always some loss of energy from the sill to infinity. Since the origin has been excluded from the region designated as the ocean, the scattered wave may be represented by (9) with A_n equal to zero. This eliminates Hankel functions of the second kind, which represent waves travelling inwards towards the origin, and leaves

$$(\phi_s)_c = f_1(z)\,e^{-i\sigma t}\sum_{n=0}^{\infty}B_n H_n^{(1)}(K_1 r)\cos n\theta, \tag{14}$$

which represents outward-travelling waves. The subscript s refers to the scattered wave and henceforth the superscript (1) will be dropped for convenience.

The potential function for the waves over the sill is (10):

$$(\phi_f)_c = f_2(z)\, e^{-i\sigma t} \sum_{n=0}^{\infty} A_n J_n(K_2 r) \cos n\theta, \tag{15}$$

where the subscript 2 refers to the region $0 \leqslant r \leqslant R$ and the subscript f refers to the waves over the sill.

5.1. *The response coefficients A_n and B_n*

The matching condition of a continuous instantaneous energy flux at the sill edge is

$$\int_{-h_1}^{0} P_1 \mathscr{U}_1 \, dz|_{r=R^+} = \int_{-h_2}^{0} P_2 \mathscr{U}_2 \, dz|_{r=R^-}, \tag{16}$$

where $\mathscr{U}_j = \partial\phi_j/\partial r$ $(j = 1, 2)$ is the radial particle velocity and

$$\phi_1 = \mathscr{R}\{(\phi_i)_c + (\phi_s)_c\}, \quad \phi_2 = \mathscr{R}\{(\phi_f)_c\},$$

$\mathscr{R}\{z\}$ designating the real part of z.

The variable part of the pressure, P_j $(j = 1, 2)$, is obtained from $(4a)$:

$$P_j = -\rho\left\{\frac{\partial\phi_j}{\partial t} + \frac{c}{h_j}(\phi_j)_b\right\}.$$

Equation (16) is an equation involving the sum of two linearly independent functions of time plus a constant term; by equating coefficients of like functions on either side of the equals sign, three equations result. Only two of these (along with two from the surface matching condition) are required to determine the complex constants A_n and B_n. Calculations carried out by Pite (1973) for a shelf model show that using the two equations involving the coefficients of the time-dependent functions yields a solution for the transmitted and reflected waves which conserves the time-averaged energy flux or equivalently satisfies the third equation.

Owing to the periodicity of the functions in (16) it is easily proved that, instead of the lengthy process of taking the real part of $(\phi_j)_c$ and then calculating the products in this equation and integrating, what could be done is to use the complex-valued potential function in place of ϕ_j, calculate the products, integrate and equate real and imaginary parts. This gives two equations identical with those found from the time-dependent terms of (16). The equations corresponding to the continuous energy flux condition (16) are those obtained by equating real and imaginary parts of

$$f_1 \sum_{n=0}^{\infty} \sum_{m=0}^{\infty} (\epsilon_n i^n J_n(K_1 R) + B_n H_n(K_1 R))\,(\epsilon_m i^m J'_m(K_1 R) + B_m H'_m(K_1 R)) \cos n\theta \cos m\theta$$
$$= f_2 \sum_{n=0}^{\infty} \sum_{m=0}^{\infty} A_n A_m J_n(K_2 R)\, J'_m(K_2 R) \cos n\theta \cos m\theta, \tag{17}$$

where
$$f_j = \int_{-h_j}^{0} f_j K_j \left\{i\sigma_j f + \frac{c}{h_j}(f_j)_b\right\} dz$$

and
$$\mathscr{C}'_n(K_j R) = d\mathscr{C}_n(K_j R)/d(K_j R),$$

$\mathscr{C}$ being any of the above cylindrical functions. The condition of a continuous surface elevation at $r = R$ is

$$[\eta_i + \eta_r]_{r=R^+} = \eta_f|_{r=R^-},$$

or that $$\sum_{n=0}^{\infty} (\epsilon_n i^n J_n(K_1 R) + B_n H_n(K_1 R)) \cos n\theta = \sum_{n=0}^{\infty} A_n J_n(K_2 R) \cos n\theta.$$

Equating the nth components at $r = R$ gives

$$\epsilon_n i^n J_n(K_1 R) + B_n H_n(K_1 R) = A_n J_n(K_2 R). \tag{18}$$

Using the right-hand side of (18) in (17) and rearranging yields

$$\sum_{n=0}^{\infty} \sum_{m=0}^{\infty} A_m J_m(K_1 R) \left\{ \frac{f_1}{f_2} (\epsilon_n i^n J_n'(K_1 R) + B_n H_n'(K_1 R)) - A_n J_n'(K_2 R) \right\} \cos n\theta \cos m\theta = 0,$$

which may be factorized into a term depending only on n and one depending only on m. That is,

$$\sum_{m=0}^{\infty} A_m J_m(K_2 R) \cos m\theta \sum_{n=0}^{\infty} \left\{ \frac{f_1}{f_2} (\epsilon_n i^n J_n'(K_1 R) + B_n H_n'(K_1 R)) - A_n J_n'(K_2 R) \right\} \cos n\theta = 0.$$

Since A_m is not in general equal to zero, it follows that

$$f_1 f_2^{-1} (\epsilon_n i^n J_n'(K_1 R) + B_n H_n'(K_1 R)) - A_n J_n'(K_2 R) = 0. \tag{19}$$

The above equation along with the nth component of the surface matching condition gives a linear system of equations in two unknowns.

Using the relation that for any argument X

$$J_n'(X) H_n^{(1)}(X) - J_n(X) H_n^{(1)\prime}(X) = -2i/\pi X,$$

it follows immediately that

$$A_n = \frac{f_1}{f_2} \frac{2\epsilon_n i^{n+1}}{\pi K_1 R (f_1 f_2^{-1} J_n(K_2 R) H_n'(K_1 R) - H_n(K_1 R) J_n'(K_2 R))} \tag{20}$$

and

$$B_n = \epsilon_n i^n \frac{J_n(K_1 R) J_n'(K_2 R) - f_1 f_2^{-1} J_n(K_2 R) J_n'(K_1 R)}{f_1 f_2^{-1} J_n(K_2 R) H_n'(K_1 R) - H_n(K_1 R) J_n'(K_2 R)}. \tag{21}$$

The ratio $f_1 f_2^{-1}$ is found to be

$$\frac{K_2^2 \sinh^2 K_2 h_2}{K_1^2 \sinh^2 K_1 h_1} \left(\frac{2K_1 h_1 + \sinh 2K_1 h_1 + i4c(\sigma h_1)^{-1} \sinh K_1 h_1}{2K_2 h_2 + \sinh 2K_2 h_2 + i4c(\sigma h_2)^{-1} \sinh K_2 h_2} \right),$$

which reduces to the ratio of the group velocities when friction is neglected. For frictionless long waves the response coefficients A_n and B_n are identical with those found by Longuet-Higgins (1967).

That A_n must remain finite can be seen from the following argument. B_n has an upper bound of ϵ_n, otherwise more energy would be leaving the sill than arriving at it and the amplitude of the oscillations over the sill would diminish with time contrary to the steady-state solution. If $A_n \to \infty$ then the bracketed term in the denominator of (20) must vanish. This is clearly impossible since the denominator of (21) would vanish too and unless the numerator was also zero the physically unacceptable result $B_n \to \infty$ would emerge. The numerator and denominator of (21) cannot vanish simultaneously owing to the placement of the zeros of the cylindrical functions.

The amplitude of the wave over the sill adjusts itself until the energy lost to infinity is just balanced by that arriving from the incident wave. To gain this balance when the sill edge lies near a nodal circle, i.e. when $J_n(k_2 R)$ is small, requires a larger response

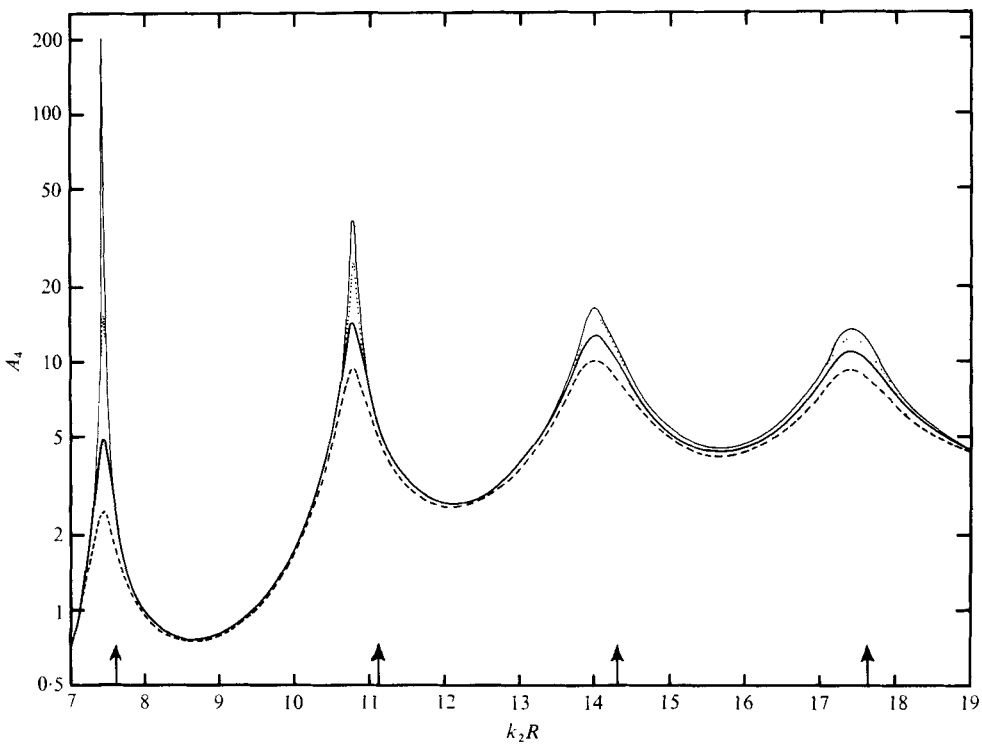

FIGURE 2. The magnitude of the response coefficient A_4 for various values of the friction constant. ——, $c = 0$; · · · · ·, $c = 3{\cdot}84$ mm/s; ▬▬, $c = 12{\cdot}1$ mm/s; – – – –, $c = 25{\cdot}4$ mm/s. The zeros of $J_4(k_2R)$ are shown by vertical arrows. $h_2/h_1 = \frac{1}{16}$, $R/h_2 = 3{\cdot}75 \times 10^3$.

coefficient over the sill than when the sill edge is such that the $J_n(k_2R)$ part of the wave amplitude is comparatively large. A similar result is seen in the large tidal amplification produced in channels open to the ocean at one end with lengths $\frac{1}{4}(2m+1)L$ such that the open end corresponds to a node. A comparison of the positions of the maxima for $|A_4|$ with the corresponding zeroes of $J_4(k_2R)$ is shown on figure 2.

The zeros of $J_n(k_2R)$ are interlaced and, for reasonably large values of the argument, separated by approximately π. Therefore in the interval between k_2R and $k_2R+\pi$, $J_0(k_2R), J_1(k_2R), J_2(k_2R), \ldots, J_{m-1}(k_2R)$ will all have zeros but higher-order functions will have no zeros. Thus, since the values of k_2R which produce maxima for A_n lie near zeros of $J_n(k_2R)$ there will be at most m maxima for A_n in the interval. It is not necessary that there be m maxima corresponding to the m zeros in the interval; this is a consequence of the modulus of the Hankel functions becoming large when the order of the function is increasingly greater than its argument k_1R. Thus the denominator in (20) becomes large and A_n is small. Since the phases of $A_nJ_n(k_2r)$ for different n are generally different, the sum of the responses at a given frequency will mask the individual behaviour of the separate components. This will not be the case for the smaller values of k_2R, where only a few zeros producing widely separated maxima are found in a relatively wide frequency band.

As in any resonating system, the effect of a dissipative friction force will be to reduce the Q-factor of the resonance peak and, for a given amount of friction, this reduction will be proportionately greater for the sharp, high-Q modes than for the ones with a

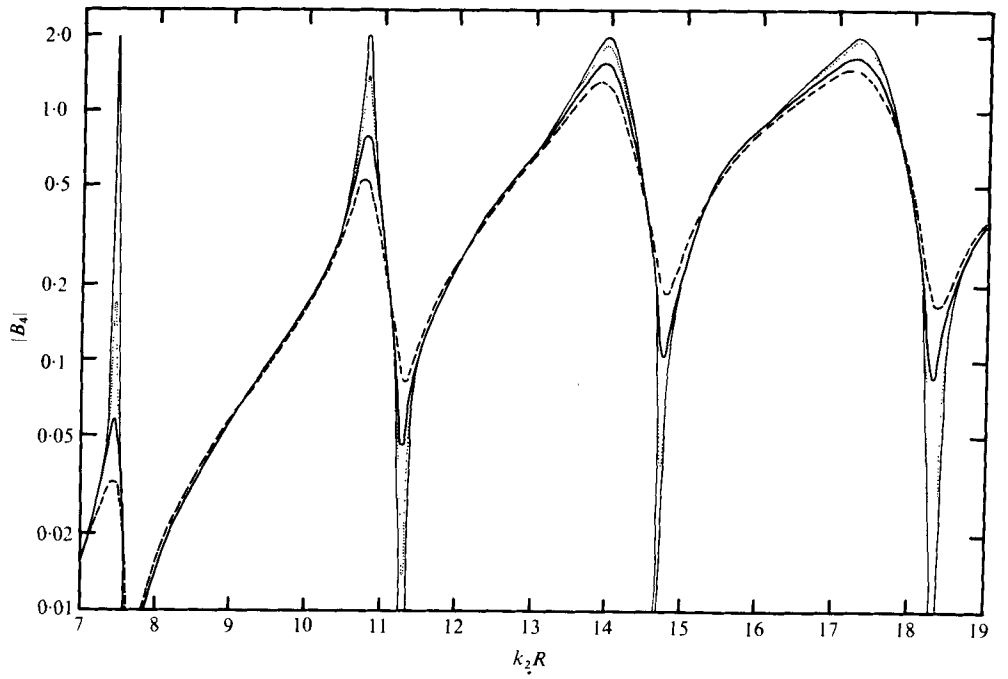

FIGURE 3. The magnitude of the response coefficient B_4 for various values of the friction constant. Curves as in figure 2. $h_2/h_1 = \frac{1}{16}$, $R/h_2 = 3{\cdot}75 \times 10^3$.

lower Q-factor. For the scattered wave in this model it is not expected that the coefficient $|B_n|$ will attain either of its extreme values of ϵ_n or zero because of energy losses over the sill. Figure 2 shows the effects of friction on $|A_4|$, which indicate that, in a physical situation where friction is important, the less highly tuned modes will be dominant and the highly tuned modes will have only a small effect on the surface configuration over the sill. The response coefficient $|B_4|$ is plotted on figure 3 and again there is a considerable smoothing of the peaks and troughs.

The value of c determined here is useful only in the laboratory case and it is of some interest to apply the theory to oceanographical scales. A linearized friction coefficient of 2·4 mm/s was obtained by Weenink (1958) for tidal waves with periods in excess of a few hours while using the data of Iwagaki & Kakinuma (1967) a value of about 51 mm/s was obtained for ocean swell with periods ranging from 10 to 20 s. In view of these values a reasonable intermediate estimate for c, for the periods used in figures 2 and 3, would be in the neighbourhood of 13 mm/s. Figures 2 and 3 show the responses over a range of values of c which includes oceanographical as well as laboratory values.

From a practical standpoint what is of interest is not so much what the surface configurations of the individual components are at any given time but rather what the extremes in the surface elevation are. These were found by obtaining, for a given r and θ, a sum for the complex series representing the instantaneous surface profile over the sill and then taking the modulus of this expression to find the amplitude of oscillation. When finding the modulus of the expression representing the waves in the ocean it proved convenient to describe the incident wave in Cartesian co-ordinates instead of using the slowly converging series in (13). In any practical calculation it is necessary to terminate the series after a given number of terms. An estimate of the number of

terms can be made by determining the order of the function that gives a rank 1 zero $j_{n,1}$ near to the value of k_2R that is of interest such that $j_{n+1,1}$ and zeros of higher order do not exist near this value. This order may be determined by use of the approximate relation for zeros of large order (Abramowitz & Stegun 1964, p. 371):

$$j_{n,1} \simeq n + 1{\cdot}86n^{\frac{1}{3}} + 1{\cdot}03n^{-\frac{1}{3}} + \ldots . \tag{22}$$

6. Experimental equipment

6.1. *The wave tank and wave generation*

A shallow 3·05 by 6·10 m tank of depth 15 cm was constructed to investigate surface waves travelling in any direction. Two 2·55 m by 1·90 m glass plates supported on all edges and levelled to $\pm 0{\cdot}02$ mm were used for the bottom of the model region. The remainder of the tank bottom was constructed of steel sheeting; this region was used for wave generation and absorption. This wave tray was supported 1·5 m off the floor by a sturdy iron channel base set on steel columns. An instrument carriage was constructed such that the wave probe could be moved to any position in the wave tank. A movable gantry was built and isolated from the tank; thus any vibrations set up while making adjustments in the model area were not transmitted to the wave tank.

The wave generator was of the piston type and consisted of a heavy steel plate machined to a close fit to the bottom and sides of the wave tank. This paddle was mounted on a rigid frame which in turn was supported by ball races running in grooved tracks to allow horizontal motion of the paddle. Oscillatory motion of the wave paddle was accomplished by use of a variable-speed rotary drive connected to the wave paddle by means of an adjustable eccentric and long connecting yoke. Adjustment of the degree of eccentricity determined the wave height and a yoke long compared with the degree of eccentricity ensured nearly simple harmonic motion. The variable-speed drive was mounted on a platform isolated from the wave tank to reduce mechanical vibration.

A gear cog was mounted on the output shaft of the variable-speed drive; a set of automotive breaker points were set such that they opened and closed as the gear cog rotated. The number of times they opened and closed in a fixed time interval was recorded electronically by a digital counter. The average period of oscillation could then be accurately determined by knowing the number of teeth on the cog, the time interval and the number of impulses to the counter.

6.2. *The wave absorber*

By far the greatest difficulties with this type of experiment, where an infinite ocean is assumed in all directions, are first the elimination of reflexions from anything but the model itself and second the production, in the model area, of a plane wave with constant height along its crest. These difficulties are not independent of one another in that it was relatively simple to design absorbers around the tank such that all reflected amplitudes were less than about 8 % of the incident amplitude, but this generally rendered a poor quality incident wave. On the other hand, if the wave absorbers were removed from all but the end of the tank an undistorted incident wave was obtained in the model area, but this was unsatisfactory since it led to the waves from the model area being reflected off the sides of the tank. Rubberized horsehair was

found to be a satisfactory material for the wave absorbers; as well as being a good absorber of wave energy it has the advantage of being readily available in 5 cm thick sheets and of being easily cut into any desired shape. All tests on the absorbers were done in a water depth of 3·36 cm, which corresponded to the depth used in the actual experiments.

It was found that, by cutting the horsehair sheets into the form of a saw tooth to reduce their frontal area, it was possible to reduce the amplitude reflexion coefficient from the value of about 30 % obtained when the waves were incident on a straight-line horsehair absorber to a value of 8 % or less. This type of reduced frontal area absorber is similar to that used in acoustical laboratories and was used down-wave of the model area in the experiments. Up-wave of the model area this type of design could not be used successfully. Incident waves travelling parallel to the ends of the saw-toothed absorber situated on the sides of the tank produced unwanted disturbances in the form of secondary waves travelling across the tank. It was thus necessary to have parallel sides perpendicular to the wave crests in this region. For wave periods of about 1 s or greater horsehair sheets with plane sides were used whereas for periods less than this it was found that the horsehair acted as a source for secondary waves which travelled across the tank. For these shorter periods it was found necessary to dispense with any absorption along the sides of the tank up-wave of the model area and to use two impervious wave guides running perpendicular to the wave crests and situated a distance apart which was slightly less than that of the absorbers down-wave of the model. A set of baffles was situated near the end of the wave guides to reduce the end effect of these guides. Thus a wave generated by the wave paddle travelled between the two parallel sides until it came to the model area; here the width of the water surface was greater and it was found that only small secondary disturbances were created by the saw-tooth absorbers in this area. Wave energy incident obliquely onto the wave guides from the model area underwent multiple reflexions from the guides and eventually reached the up-wave end of the tank and was absorbed by the wave absorber situated in front of the wave paddle.

The absorber in front of the paddle must allow waves generated from the paddle to travel through it with as little distortion as possible and must be able to absorb efficiently waves incident from down-wave of the wave paddle. The waves generated by the wave paddle will be reduced in height as they travel across this absorber, but, by adjusting the height of the generated wave, the absorption can be compensated for and the desired incident wave height produced. It is clear that this absorber must have equal absorption along its length to keep distortion of the incident wave to a minimum. This immediately excludes a saw-tooth type of absorber and for periods less than about 1 s a strip of horsehair with parallel sides also proved too asymmetric. It was found that 1·25 cm diameter glass marbles tightly packed in a single layer 1·2 m wide across the tank proved to be an adequate absorber and allowed for a relatively undistorted incident wave. A plane wave incident normally from the model area on the wave paddle was found to be reduced in amplitude by 87 % after crossing and recrossing the marble absorber. Figure 4 shows a typical arrangement of absorbers in the tank.

6.3. *The wave probe*

The wave heights were measured by using a micrometer resistance-type wave probe of the same design as that described by Wong, Ippen & Harleman (1963). Basically its

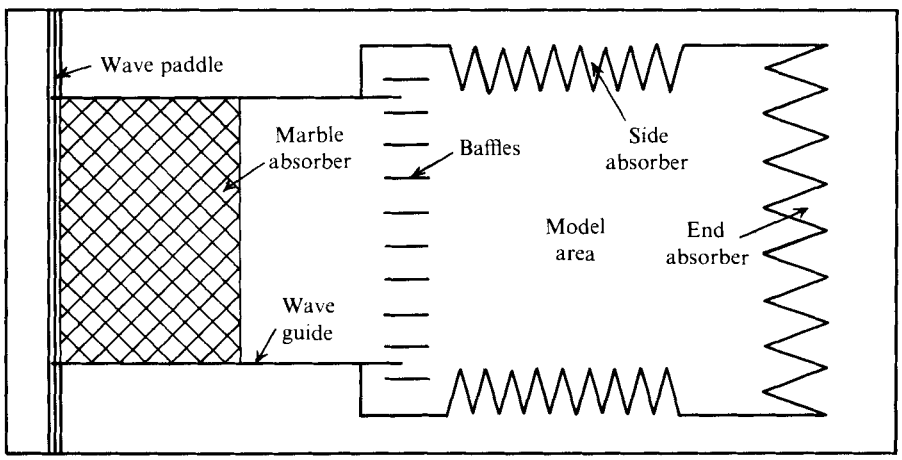

FIGURE 4. Schematic diagram of the wave-absorber arrangement for 0·5 s $\leqslant T \leqslant$ 0·8 s.

principle of operation was that as the depth of immersion of two vertical wires in a conducting fluid changed, the electrical resistance between them changed; this change in resistance was detected by use of a high frequency strain gauge bridge in conjunction with an ultra-violet recording system. Unfortunately, this direct method proved somewhat unreliable owing to extraneous changes in the resistance between the two sensing wires and to the effect of the meniscus. To eliminate partially this unreliability the experimental wave height was compared with a standard wave height recorded as soon as possible after the experimental measurement was taken. This standard was produced by driving the thimble of the micrometer in circular oscillatory motion by use of an oscillatory drive coupled to the micrometer by a set of gear cogs. The motion of the micrometer was transmitted to the sensing wires in the form of a vertical oscillatory motion whose amplitude could be read off the micrometer scale and compared with the output obtained from the recording system.

The results are plotted in figure 5 and show a linear relationship between the recorded and actual amplitudes. With a fixed amplitude of motion and using different periods of oscillation there was found to be a variation in the recorded output. Thus it was necessary to ensure that the 'standard wave' and the experimental wave had the same frequency or to make a suitable correction to one of them. This variation was the same for all amplitudes tested and was caused by a nonlinear response in the bridge–recording circuit.

The actual experimental wave height was then

$$H = (H_{\mathrm{exp}}/H'_c)\, d,$$

where H_{exp} is the recorded experimental wave height, H'_c is the recorded standard wave height correct to the same period as H_{exp} and d is the actual distance that the probe wires oscillated to obtain the standard. Experience showed that wave heights of 0·05 mm or less could be measured with a repeatability of within 5 %; larger waves had, in general, a greater degree of repeatability. The major shortcoming of this procedure was the necessity, after taking each experimental measurement, of stopping the wave generator, waiting until the water surface became undisturbed and then taking a measurement for the standard. Owing to the spacing of the sensing wires (6·3 mm), the

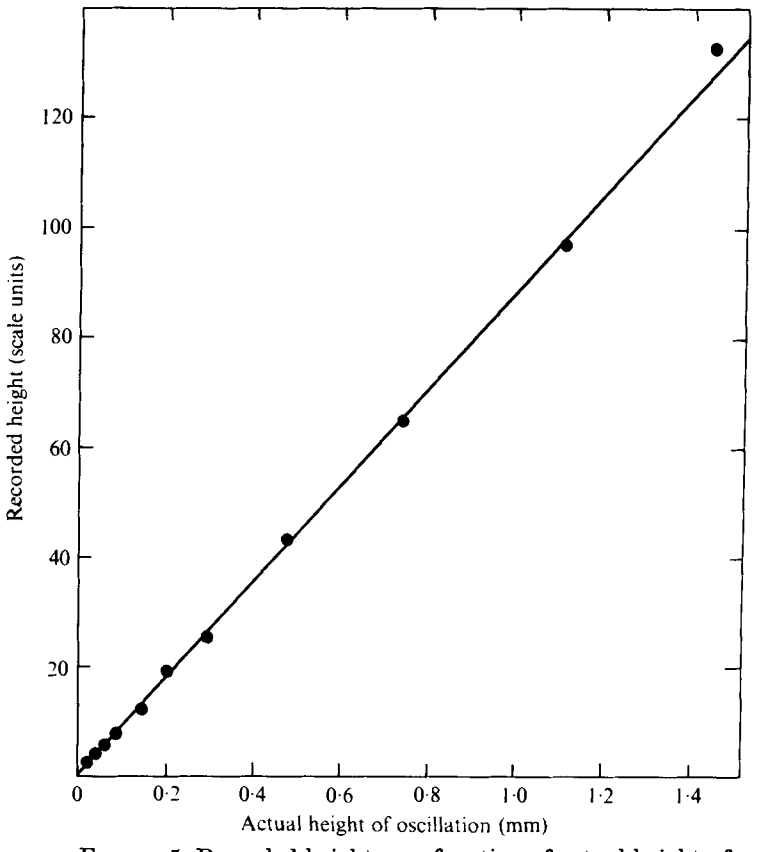

FIGURE 5. Recorded height as a function of actual height of oscillation of the sensing wires.

measured wave heights did not correspond to a point measurement but to the average of the heights existing at each sensing wire.

7. Experimental verification of the amplification and scattering of waves by a submerged circular sill

In this section the experimental verification of some of the results in § 5 is described. Basically two experiments were undertaken, the first being the measurement of the wave profile over the sill at a fixed position using a variable wave period and the second the measurement of the surface profile at various positions for a fixed wave period. An experiment was also run to determine values for the friction constant used in the theoretical development.

In all experiments involving the ocean and circular sill the depth in the ocean was set at 3·36 cm and that over the sill at 0·84 cm. This did not give as high a depth ratio as was desired but it proved too difficult to absorb the waves successfully if the depth of the ocean was increased greatly. A reduction of the depth over the sill gave problems with second-order effects caused by the relatively large wave amplitudes generated over the sill by the incident waves. The incident wave was typically 0·1–0·25 mm in height, which produced waves of at most two or three times this size over the sill.

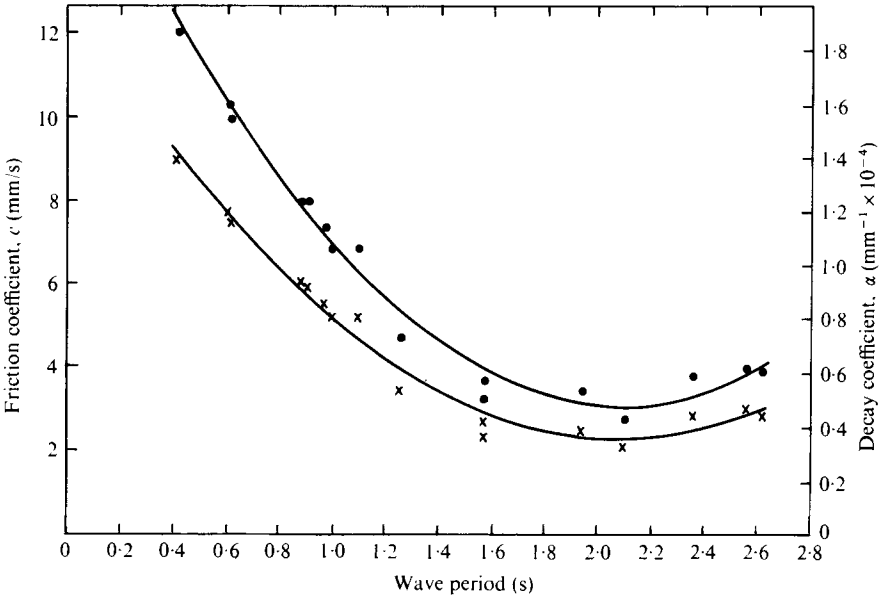

FIGURE 6. The decay coefficient (circles) and friction coefficient (crosses) as a function of the wave period for tap water with $h = 0{\cdot}84$ mm.

A circular sill was constructed from a flat steel plate 45·7 cm in diameter and 2·54 cm thick; this plate was surface ground such that its thickness was constant to within 0·025 mm. The water depth was measured, using a vernier point gauge, by taking the difference in readings between when the point just made contact with the water surface and when it was in contact with the bottom. Several depth measurements were taken and averaged over the sill and in the deeper water. These measurements were accurate to about $\pm 0{\cdot}4$ mm for the deeper water and to about $\pm 0{\cdot}2$ mm for that over the sill. The greater accuracy over the sill was possible because the model had a very precise thickness whereas the glass plate, although on average quite flat, had small irregularities in its surface.

7.1. *The linear friction constant*

The circular sill was removed from the tank for the experiment to determine the friction constant and the water depth set to 0·84 cm. Waves of a fixed period were generated in the tank and their heights were measured at intervals along the wave tank. To eliminate the possibility of errors caused by the reflexion (although small) from the end of the tank, the wave paddle was started from rest and a recording made of the transient and steady-state waves generated. It was found that after two or three cycles a steady state was reached. The wave heights were plotted against distance on semi-log paper and from the resulting straight line a value of the decay coefficient α was deduced.

Equations (11) and (12) form a pair of nonlinear equations in the two unknowns, namely k and c. These equations were solved numerically for a given wave period, water depth and experimentally determined decay coefficient.

A variety of values for α were determined using wave periods ranging from 0·4 to 2·6 s and corresponding values for c calculated. The results are plotted in figure 6;

the solid lines designate a least-squares polynomial fit to the points and it was this polynomial that was used to calculate c for the experiments involving the circular sill. Linear boundary-layer solutions (Biesel 1949) show that the decay coefficient should vary as $T^{-\frac{1}{2}}$; these experiments revealed a stronger dependence on T than that predicted. As found by a number of authors (for example Iwagaki, Tsuchiya & Chen 1967) the predicted values for the decay coefficient were considerably lower than the experimental ones.

The value for c found above was used for the other fluid depth of 3·36 cm; this was justified first in that it is not expected that the fluid depth will appreciably affect the amount of energy lost in the thin layer near the bottom and second by experimental verification carried out by Pite (1973). Any dissipation at the free surface by the formation of a surface film was found to be negligible. This was established by thoroughly mixing the fluid to break up any surface film at the free surface and then measuring the wave heights at a fixed point at regular time intervals. This procedure was carried out for both water depths and no variation in the wave amplitude with time was found. This result is in agreement with theoretical work of Van Dorn (1966) that showed the surface dissipation to be much less than the bottom dissipation when reasonably long waves were used.

7.2. *Measurement of the surface profile over the sill for various wave periods*

The surface probe was set at a fixed position over the sill and wave heights were measured for a variety of wave periods using a fixed amplitude of motion of the wave paddle. The circular sill was then removed from the tank and wave heights were measured at a few positions in $r < R$ with the probe situated along the $\theta = \frac{1}{2}\pi$ line. These measurements, when averaged for each period, corresponded to the incident wave height. The wave heights H_f measured over the sill were compared with the height H_i of the incident wave of the same period.

The ratio H_f/H_i of these two heights gave the surface response over the sill to a forcing wave of unit amplitude. These results are shown graphically in figure 7 and compared with the theoretical predictions calculated using (20); the friction constant for the various wave periods was calculated from the empirical relation determined experimentally in § 7.1. There appears to be reasonably good agreement between the experimental results and those predicted by the theory. For comparison, the theoretical results when friction is neglected are also plotted on figure 7. The build-up of the wave height over the sill corresponding to the maximum at about $k_2 R = 4{\cdot}2$ is shown in figure 8 (a) and the reduction in wave height corresponding to the minimum at about $k_2 R = 5{\cdot}5$ is shown in figure 8 (b). These figures reveal that a steady-state wave height was reached after about 8 or 10 cycles.

7.3. *Measurement of the surface profile at different radii using a constant wave period*

Using a constant wave period and a fixed value of the angle θ, wave heights were measured at various radii over the sill and in the ocean. The sill was then removed from the tank and the wave heights were measured along the $\theta = \frac{1}{2}\pi$ line; an average of these results was taken to give the incident wave height. The variation in wave height across the tank was generally less than $\pm 5\,\%$ from this average and was attributed to

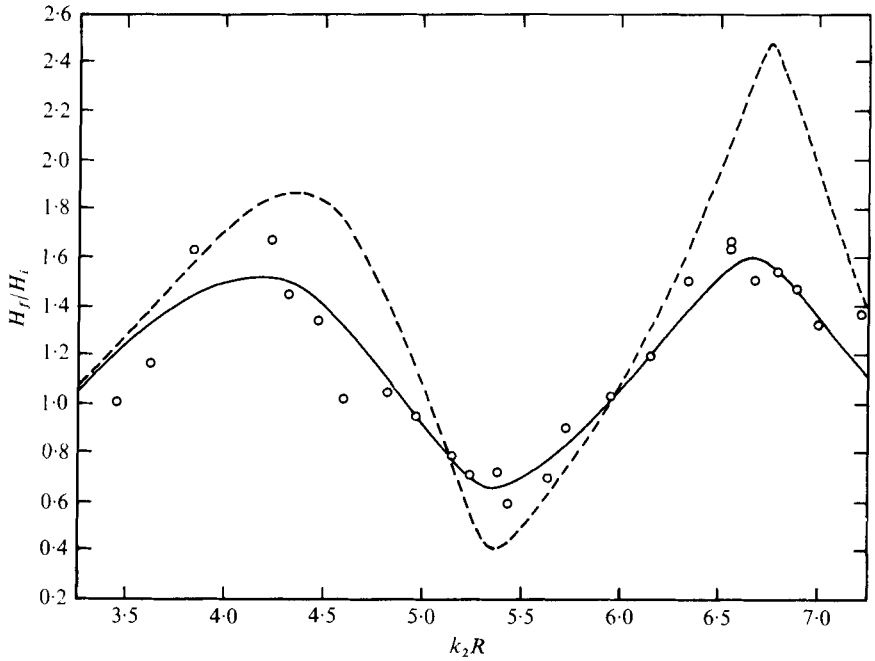

FIGURE 7. The variation of the relative wave height H_f over the sill as a function of the dimensionless frequency k_2R (relative to a forcing wave of height $= H_i$). ○, experimental; ——, theoretical with c as determined experimentally; – – – –, theoretical with $c = 0$. $r/R = 21$, $\theta = \frac{1}{2}\pi$, $h_2/h_1 = \frac{1}{4}$, $R/h_2 = 27$.

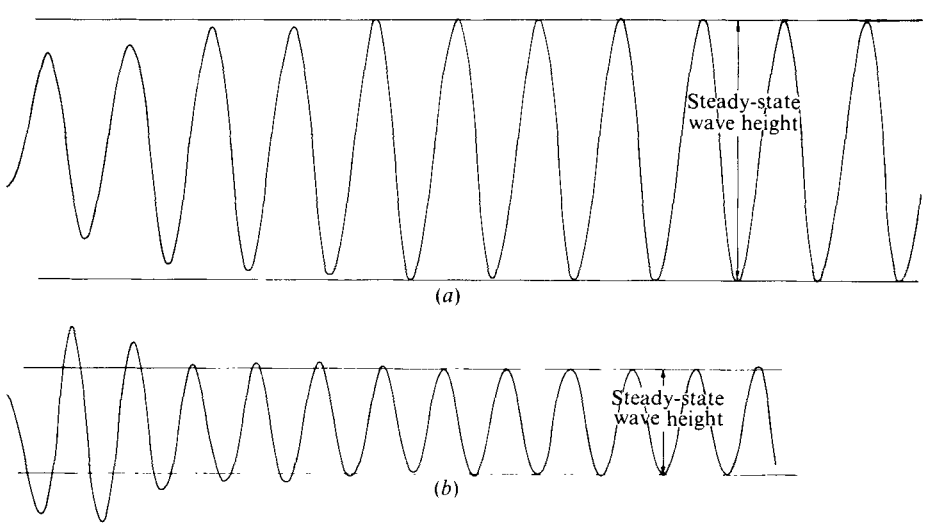

FIGURE 8. Wave profile showing (*a*) the build-up and (*b*) the reduction of wave height over the sill with parameters as in figure 7 and (*a*) $k_2R \simeq 4{\cdot}2$, (*b*) $k_2R \simeq 5{\cdot}5$.

interference effects from secondary waves incident from the absorbers. See Pite (1973, figures *A*7.5*A* and *A*7.5*B*).

The wave heights measured with the sill in place were compared with the average incident wave height to give the ratios H_f/H_i over the sill and H_s/H_i in the ocean. These results are shown in figures 9(*a*), (*b*) and (*c*) for wave periods of 2·37 s ($k_2R = 2{\cdot}08$),

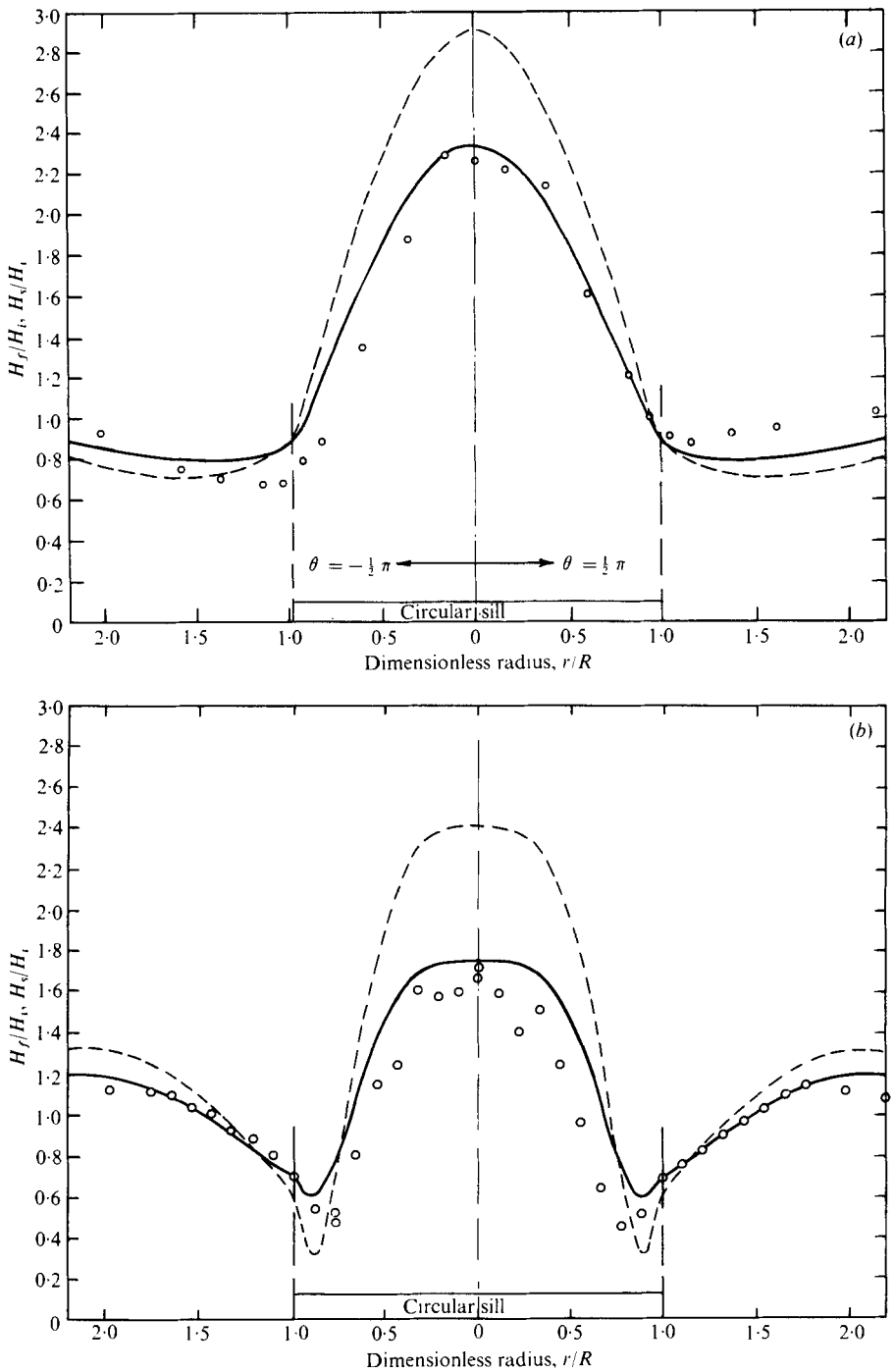

FIGURES 9(*a*, *b*). For legend see facing page.

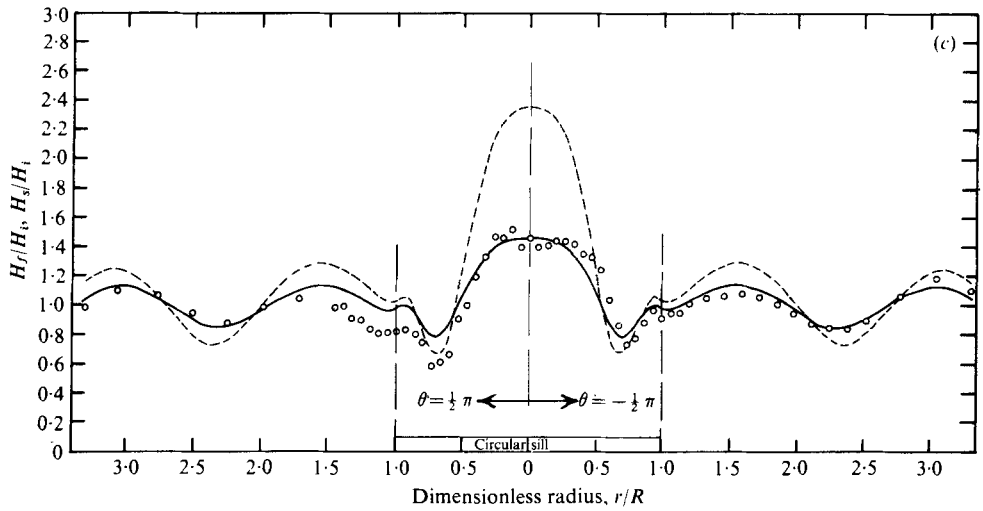

FIGURE 9. The relative height of the waves in the ocean and over the sill for (*a*) $T = 2{\cdot}37$ s ($k_2R = 2{\cdot}08$), (*b*) $T = 0{\cdot}977$ s ($k_2R = 5{\cdot}15$) and (*c*) $T = 0{\cdot}604$ s ($k_2R = 8{\cdot}40$) (relative to a forcing wave of height $= H_i$). ○, experimental; ——, theoretical with c as determined experimentally; – – – –, theoretical with $c = 0$. $h_2/h_1 = \frac{1}{4}$, $R/h_2 = 27$, $h_2 = 0{\cdot}84$ mm.

	$T = 2{\cdot}37$ s ($k_2R = 2{\cdot}08$)		$T = 0{\cdot}977$ s ($k_2R = 5{\cdot}15$)		$T = 0{\cdot}604$ s ($k_2R = 8{\cdot}40$)	
n	$\lvert A_n\rvert$	$\lvert B_n\rvert$	$\lvert A_n\rvert$	$\lvert B_n\rvert$	$\lvert A_n\rvert$	$\lvert B_n\rvert$
0	2·338	0·540	1·749	0·651	1·455	0·479
1	2·450	0·815	2·496	1·171	2·252	1·278
2	1·226	0·141	3·525	1·231	2·896	1·023
3	0·522	0·006	3·107	1·149	2·493	0·404
4	0·242	0·000	0·903	0·153	2·392	0·377
5	0·116	0·000	0·305	0·012	2·799	0·775
6	0·057	0·000	0·125	0·001	1·569	0·329
7	0·028	0·000	0·055	0·000	0·339	0·028
8	0·013	0·000	0·025	0·000	0·113	0·002
9	0·001	0·000	0·012	0·000	0·045	0·000

TABLE 1. The theoretical response coefficients used to calculate the surface profile for parameters corresponding to experimental conditions.

0·977 s ($k_2R = 5{\cdot}15$) and 0·604 s ($k_2R = 8{\cdot}40$) respectively. The theoretical results are in reasonably good agreement with the experimental ones. The rather large discrepancy near the left-hand side of the sill edge on figure 9(*c*) is a consequence of the incident wave in this region having a somewhat lower height, due to interference from secondary waves from the absorbers, than those of the average. Although the results are low in this region, the variation in height with radius agrees well with the theoretical variation.

The theoretical curves when friction is neglected are also drawn on these figures and indicate a much larger range of wave heights than was found experimentally or theoretically when friction was included. Table 1 lists the response coefficients $|A_n|$ and $|B_n|$ corresponding to the wave periods given above and shows that for $T = 2{\cdot}37$ s only the lowest modes are of importance whereas the higher-order modes gain importance as T decreases.

8. Conclusions

The response coefficients over a submerged circular sill subject to the diffraction of a plane wave from the ocean were found using the matching conditions at the depth discontinuity of a continuous surface streamline and a continuous energy flux. Physical arguments indicated that the nth response coefficient over the sill should be a maximum when the sill edge was near a zero of $J_n(k_2R)$; numerical calculations showed this to be the case. Therefore as the radius of the sill becomes progressively smaller compared with the wavelength fewer and fewer modes are present over the sill. The effect of friction was to reduce the response coefficient over the sill and this reduction was found to be proportionately greater for the high-Q modes than for the less sharp ones. A reduction in magnitude of the peaks and troughs corresponding to the response coefficient in the ocean was found and, again, this reduction was greatest for the more sharply tuned modes; $|B_n|$ no longer reached its extreme values of zero and ϵ_n.

Since the zeros of $J_n(k_2R)$ are interlaced and, for a given n with k_2R sufficiently large, are separated by approximately π, in a relatively narrow frequency band there will be many resonant modes present. With regard to the effect of friction on $|A_n|$ and to the fact that each mode generally has a different phase from any other it is unlikely, at the higher frequencies, that any single mode will be dominant over the rest. This is not the case at lower frequencies, where only the lower modes are present and their resonant peaks do not overlap greatly.

This theory of wave diffraction with damping over a circular sill was verified in two experiments. In the first all parameters were held fixed and the wave period was varied while in the second the position of measurement was varied along a radius with the period constant. The results agree quite well with the theoretical ones and show a large difference from those predicted by frictionless theory.

REFERENCES

Abramowitz, M. & Stegun, I. A. (eds.) 1964 *Handbook of Mathematical Functions.* Washington: Nat. Bur. Stand.

Bartholomeusz, E. C. 1958 The reflection of long-waves at a step. *Proc. Camb. Phil. Soc.* **54**, 106–118.

Biesel, F. 1949 Calculation of wave damping in a viscous liquid of known depth. *Houille Blanche* **4**, 630–634.

Hilaly, N. 1967 Diffraction of water waves over bottom discontinuities. *Hydraul. Engng Lab., Univ. California, Berkeley Tech. Rep.* HEL–1–7.

Hough, S. S. 1897 On the influence of viscosity on waves and currents. *Proc. Lond. Math. Soc.* **28**, 264–288.

Ippen, A. T. (ed.) 1966 *Estuary and Coastline Hydrodynamics*, pp. 71–77. McGraw-Hill.

Ippen, A. T. & Harleman, D. R. F. 1960 Analytical study of salinity intrusion in estuaries and canals. *Comm. Tidal Hydraul., Corps Engrs, Vicksburg, Mississippi.*

Iwagaki, Y., Tsuchiya, Y. & Chen, H. 1967 On the mechanism of laminar damping of oscillatory surface waves due to bottom friction. *Bull. Disaster Prevention Res. Inst.* **16**(3), 49–75.

Iwagaki, Y. & Kakinuma, T. 1967 On the bottom friction factors off five Japanese coasts. *Coastal Eng. Japan* **10**, 13–22.

Lamb, H. 1932 *Hydrodynamics*, 6th edn, pp. 262–263. Cambridge University Press.

Le Mehaute, B. 1960 Periodic gravity waves at discontinuity. *J. Hydraul. Div., Proc. A.S.C.E.* **86**, 11–41.

LI, H. 1954 Stability of oscillatory laminar flow along a wall. *U.S.A. Beach Erosion Bd Tech. Memo.* no. 47, pp. 1–48.

LONGUET-HIGGINS, M. S. 1967 On the trapping of wave energy round islands. *J. Fluid Mech.* **29**, 781–821.

MILES, J. W. 1967 Surface wave scattering matrix for a shelf. *J. Fluid Mech.* **28**, 755–767.

NEWMAN, J. N. 1965 Propagation of water waves over an infinite step. *J. Fluid Mech.* **23**, 399–415.

PITE, H. D. 1973 Studies in frictionally damped waves. *Water Res. Lab., Univ. New South Wales Rep.* no. 138, pp. 46–56, A7–5, 102–104.

SMITH, R. & SPRINKS, T. 1975 Scattering of surface waves by a conical island. *J. Fluid Mech.* **72**, 373–384.

SUMMERFIELD, W. C. 1969 On the trapping of wave energy by bottom topography. *Horace Lamb Centre Ocean. Res., Flinders Univ. Res. Paper* no. 30, pp. 3–12, 89.

VAN DORN, W. G. 1966 Boundary dissipation of oscillatory waves. *J. Fluid Mech.* **24**, 769–779.

WEENINK, M. P. H. 1958 *Meded Verk. k. ned met. Inst.* **73**, 87–88.

WONG, K. K., IPPEN, A. T. & HARLEMAN, D. R. F. 1963 Interaction of tsunami with oceanic islands and submarine topographies. *M.I.T. Hydrodyn. Lab. Tech. Rep.* no. 62, pp. 52–55.